

Article

NEXAFS and XPS Studies of Co Doped Bismuth Magnesium Tantalate Pyrochlores

Nadezhda A. Zhuk ^{1,*} , Boris A. Makeev ² , Aleksandra V. Koroleva ³ , Sergey V. Nekipelov ⁴ 
and Olga V. Petrova ⁴ 

¹ Institute of Natural Sciences, Syktyvkar State University, Oktyabrsky Prospect, 55, 167001 Syktyvkar, Russia

² Institute of Geology of the Komi Science Center UB RAS—Ural Branch of the Russian Academy of Sciences, Pervomaiskaya St. 48, 167982 Syktyvkar, Russia; makboris@mail.ru

³ Faculty of Physics, Saint Petersburg State University, University Emb. 7/9, 199034 St. Petersburg, Russia; dalika@inbox.ru

⁴ Institute of Physics and Mathematics of the Komi Science Center UB RAS, Oplesnina St. 4, 167982 Syktyvkar, Russia; nekipelovsv@mail.ru (S.V.N.); teiou@mail.ru (O.V.P.)

* Correspondence: nzhuck@mail.ru

Abstract: Co doped bismuth magnesium tantalate with a pyrochlore structure (sp. gr. Fd-3m) was synthesized for the first time using the standard ceramic method. Single phase $\text{Bi}_2\text{Mg}_{1-x}\text{Co}_x\text{Ta}_2\text{O}_9$ samples were found to be formed when $x < 0.7$ in the X-ray phase analysis. However, with a higher cobalt content in the samples, the impurity phase $\beta\text{-BiTaO}_4$ (sp. gr. P-1) is detected, and its amount is proportional to the degree of cobalt doping. The formation of solid solutions is evidenced by a uniform increase in the unit cell parameter of the Co,Mg co doped bismuth tantalate phase with an increase in the content of cobalt ions in the samples from 10.5412(8) ($x = 0.3$) to 10.5499(8) Å ($x = 0.7$). The samples exhibit a porous microstructure consisting of chaotically oriented and partially fused elongated grains measuring 1–2 μm . The dependence of the ceramic grain size on the $n(\text{Mg})/n(\text{Co})$ ratio was not determined. X-ray spectroscopy (energy-dispersive X-ray absorption structure (NEXAFS) and X-ray photoelectron spectroscopy (XPS)) was used to study the charge state of ions in $\text{Bi}_2\text{Mg}_{1-x}\text{Co}_x\text{Ta}_2\text{O}_9$. The NEXAFS and XPS data showed that doping with cobalt and magnesium did not change the bismuth and tantalum oxidation states in pyrochlore; in particular, the ions maintained their oxidation states of Bi(+3), Mg(+2) and Ta(+5). The energy position of the peaks of the Ta4f-, Ta5p-, Ta4d spectra had a characteristic shift towards lower energies compared to the binding energy in pentavalent tantalum oxide Ta_2O_5 . A shift towards lower energies is characteristic of a decrease in the effective positive charge; in particular, for the Ta4f and Ta4d spectra we presented, this energy shift was $\Delta E = 0.65$ eV, and in the region of the Ta4d edge—0.55 eV. This in turn allowed for us to assume that tantalum atoms have the same effective charge $+(5-\delta)$. The oxidation state of cobalt ions was predominantly 2+ and partially 3+, according to NEXAFS spectroscopy data.

Keywords: pyrochlore; co doping; BiTaO_4 ; XPS; NEXAFS



Citation: Zhuk, N.A.; Makeev, B.A.; Koroleva, A.V.; Nekipelov, S.V.; Petrova, O.V. NEXAFS and XPS Studies of Co Doped Bismuth Magnesium Tantalate Pyrochlores. *Chemistry* **2024**, *6*, 323–332. <https://doi.org/10.3390/chemistry6020018>

Academic Editors: Narcis Avarvari and Matthias Lehmann

Received: 13 February 2024

Revised: 19 March 2024

Accepted: 29 March 2024

Published: 3 April 2024



Copyright: © 2024 by the authors. Licensee MDPI, Basel, Switzerland. This article is an open access article distributed under the terms and conditions of the Creative Commons Attribution (CC BY) license (<https://creativecommons.org/licenses/by/4.0/>).

1. Introduction

Synthetic pyrochlores represent a significant group of materials that are in demand in various technological applications due to a wide range of practically useful properties, such as metallic and ionic conductivity, superconducting and ferroelectric properties [1,2]. They may also be characterized by ferro- and antiferromagnetism, magnetoresistance and spin glass state [3,4]. Synthetic pyrochlores have found application in solid-state devices as thin-film resistors, as thermistors and communication elements, and are promising as photocatalysts and components of ceramic molds for radioactive waste.

Complex oxides with a pyrochlore structure may be promising as a dielectric layer in multilayer ceramic capacitors, tunable microwave dielectric components, resonators and microwave devices due to their good dielectric properties that are tunable by the electric

field. They are distinguished by a low sintering temperature and chemical compatibility with low-melting silver and copper conductors [5–7]. Traditionally, the crystal structure of oxygen-containing pyrochlores is described by the general formula $A_2B_2O_7$. It contains two interpenetrating and weakly interacting A_2O' sublattices with an anti-cristobalite structure and a B_2O_6 sublattice [8,9]. The octahedrons of the B_2O_6 basic structure form a vertex-bound tetrahedral framework, the voids of which contain two large cations A and an additional atom O for each formula unit of the $(BO_3)_2$ framework. Relatively small B cations (Ti(IV), Ta(V), Nb(V)) are placed in the oxygen octahedra, while large A ions (Bi(III), Pb(II), Tl(I)) are located in a polyhedron of eight oxygen atoms of the A_2O and B_2O_6 sublattices. The wide range of cation substitutions in the A and B crystallographic positions is due to the structural flexibility of pyrochlores caused by the tolerance of the A_2O sublattice to the formation of cationic and oxygen vacancies. Therefore, along with traditional $A_2B_2O_7$ pyrochlores such as $A^{3+}_2B^{4+}_2O_7$ and $A^{2+}_2B^{5+}_2O_7$, which cationic sublattices are homogeneous and filled with ions of the same chemical nature, mixed $A_2BB'O_7$ pyrochlores with a B_2O_6 sublattice filled with different valence ions B and B' have also been found [8]. The concept of tolerance factor based on the ratio of cationic radii of ions of A_2O and B_2O_6 sublattices is widely used to describe the stability of the formed compositions. According to [8], the range of $rA/rB = 1.46$ – 1.80 values for $A^{3+}_2B^{4+}_2O_7$ and 1.40 – 2.20 for $A^{2+}_2B^{5+}_2O_7$ limits the stability of binary pyrochlores. The proposed criterion has proved to be excellent for evaluating the preservation of the pyrochlore structural type for binary oxide pyrochlores formed in $3+/4+$ or $2+/5+$ stoichiometry. Meanwhile, for mixed pyrochlores, the stability criterion has an indirect application and does not give an understanding of the maximum capacity of dopants in the pyrochlore cationic sublattices. Generally, the concentration fields of mixed pyrochlores formation are currently determined experimentally, as has been done for pyrochlores in Bi_2O_3 – MO_x – $Ta(Nb)_2O_5$ (M–Co, Ni, Mn, Fe, Cu, Zn) systems [10–12]. The mixed placement cation in two non-equivalent cationic sublattices is due to the doping of pyrochlores with heterovalent and disproportionate ions of transition 3D elements (Zn^{2+} , Mn^{2+} , Co^{2+} , Cu^{2+}). This substitution of 3D-element ions causes tension in the octahedral framework. This doping type results in the formation of a sublattice of partially vacant A cations mixed with other cations in the pyrochlore structure, resulting in the appearance of relaxation properties in the ceramics [13,14].

Bismuth-containing pyrochlores are promising for use in multilayer ceramic capacitors, resistors, resonators, microwave sensors and filters, electrocatalysts and photocatalysts, due to their excellent dielectric properties. Currently, complex oxides with a pyrochlore structure based on bismuth tantalate and niobate, doped with 3D ions, are being actively studied [15–20]. Cobalt-containing pyrochlores based on bismuth tantalate have not been studied enough. There is one known work [17] which shows that pyrochlore of the composition $Bi_{1.49}Co_{0.8}Ta_{1.6}O_{7.0}$ contains heterovalent cobalt ions Co(II) and Co(III). Similar cobalt pyrochlores based on bismuth niobate have been extensively researched over a wide range of concentrations for the Bi_2O_3 – CoO – Nb_2O_5 system [12]. The research indicates that single-phase pyrochlores have a Bi-deficient stoichiometry, in which Co(II) ions occupy 8% to 25% of the A positions. The paramagnetic atoms exhibit a weak antiferromagnetic exchange, while cobalt atoms have an effective charge of $+(2,2)$, indicating the presence of dissociated cobalt ions. In this study, we synthesized a complex Co,Mg co doped tantalate pyrochlore and investigated the effect of magnesium ions on the electronic state of ions in the pyrochlore composition, including cobalt ions, using X-ray spectroscopy.

2. Experimental Part

Samples of $Bi_2Mg_{1-x}Co_xTa_2O_9$ ($x \leq 1.0$) were synthesized using oxides of MgO, Bi_2O_3 , CoO and Ta_2O_5 via the solid-phase reaction method. The oxides were finely ground and mixed with stoichiometric proportions and pressed into disk-shaped compacts (10 mm diameter, 3–4 mm thickness). High-temperature treatment of the samples was carried out sequentially at 650 °C (15 h), 850 °C (15 h), 950 °C (15 h) and 1050 °C (15 h). At each stage of the synthesis, the samples were finely ground into powder and compacted in the form

of disks for close contact of the ceramic grains. X-ray phase analysis of the samples was carried out using a Shimadzu 6000 X-ray diffractometer (SHIMADZU CORPORATION, Kyoto, Japan) (CuK α radiation). The unit cell parameters of the samples were calculated using the software package CSD-4 [21]. The microstructure of the synthesized samples was studied using scanning electron microscopy (SEM). The local chemical composition of the samples was studied by energy dispersive X-ray (EDX) spectroscopy using a Tescan VEGA 3LMN scanning electron microscope (Kohoutovice, Czech Republic) and an INCA Energy 450 energy dispersive spectrometer (Oxford Instruments, Abingdon, UK), respectively. X-ray photoelectron spectra (XPS) were obtained using the equipment of the resource center of the Science Park of St. Petersburg State University (St. Petersburg, Russia) "Physical methods of surface research". XPS analysis was carried out on a Thermo Scientific ESCALAB 250Xi X-ray spectrometer (Waltham, MA, USA). An X-ray tube with AlK α radiation (1486.6 eV) was used as a source of ionizing radiation. The ion–electronic charge compensation system ensured the neutralization of the electrical charge of the samples. All absorption bands in the spectra were calibrated relative to the C1s peak, in which the energy position corresponds to an energy of 284.6 eV. The ESCALAB 250Xi spectrometer software, (Thermo Fisher Scientific, Great Britain, Avantage v5.9925) made it possible to process the experimental data of the samples. Studies of the samples using the near-edge X-ray absorption fine structure (NEXAFS) method were carried out at the NanofES station of the synchrotron radiation source KISS, Kurchatov Institute (Moscow). NEXAFS spectra were acquired in total electron yield (TEY) mode with an energy resolution of 0.5 eV.

3. Results and Discussion

3.1. Phase Composition of the $\text{Bi}_2\text{Mg}_{1-x}\text{Co}_x\text{Ta}_2\text{O}_9$

The X-ray phase analysis allows us to determine that the samples with the composition $\text{Bi}_2\text{Mg}_{1-x}\text{Co}_x\text{Ta}_2\text{O}_9$ ($0 \leq x < 0.7$) are single-phase and crystallize in the cubic pyrochlore structural type (sp. gr. Fd-3m) (Figure 1). When $x \geq 0.7$, in addition to the reflections of the basic cubic phase, reflections of the triclinic modification of bismuth orthotantalate (BiTaO_4 , sp. gr. P-1) are observed on the X-ray diagrams of the samples [22]. The cobalt doping amount is directly proportional to the level of BiTaO_4 impurity in the samples, which the content at $x(\text{Co}) = 0.7$ does not exceed 4 wt.%. The unit cell parameter of cubic pyrochlore in $\text{Bi}_2\text{Mg}_{1-x}\text{Co}_x\text{Ta}_2\text{O}_9$ increases uniformly with increasing cobalt ion content from 10.5412(8) ($x = 0.3$) to 10.5499(8) Å ($x = 0.7$). It is important to note that the cell parameter growth is insignificant with increasing cobalt content despite significantly larger ionic radii of cobalt(II) and magnesium compared to the radius of tantalum(V) ions ($R(\text{Co(II)})^{\text{h.s.}}_{\text{c.n-6}} = 0.745$ Å, $R(\text{Mg(II)})_{\text{c.n-6}} = 0.72$ Å, $R(\text{Ta(V)})_{\text{c.n-6}} = 0.64$ Å) [23]. Here, the symbol h.s. (high spin) denotes the high spin state of the ion, symbol c.n. (coordination number) denotes the coordination number of the ion. The cell parameter remains relatively constant due to the presence of cobalt(II) ions in the bismuth position, which have a larger ionic radius than that of Co(II) ($R(\text{Co(II)})^{\text{h.s.}}_{\text{c.n-8}} = 0.9$ Å, $R(\text{Bi(III)})_{\text{c.n-8}} = 1.17$ Å) or due to the oxidation of some cobalt(II) ions to Co(III) with a smaller ionic radius ($R(\text{Co(III)})^{\text{h.s.}}_{\text{c.n-6}} = 0.545$ Å). In all cases, it is assumed that the oxygen polyhedral environment creates a crystal field of weak to medium strength which leads to a high spin state of cobalt ions. The calculated unit cell parameters of $\text{Bi}_2\text{Mg}_{1-x}\text{Co}_x\text{Ta}_2\text{O}_9$ samples correlate well with the literature data for the $\text{Bi}_{1.6}\text{Co}_{0.8}\text{Ta}_{1.6}\text{O}_{7.2}$ (pr. gr. Fd-3m:2, $a = 10.5526(2)$ Å, $Z = 8$ (No. 227) [24] and $\text{Bi}_{1.49}\text{Co}_{0.8}\text{Ta}_{1.6}\text{O}_{7.0}$ ($a = 10.54051(3)$ Å) [17] compositions.

The calculated cell parameter is much larger than that of nickel pyrochlore based on bismuth tantalate ($a = 10.5343$ Å) [18], and on the other hand is closer to that of cobalt pyrochlores based on bismuth niobate ($a = 10.580$ – 10.556 Å) [12]. This similarity of the cell parameter of $\text{Bi}_2\text{Mg}_{1-x}\text{Co}_x\text{Ta}_2\text{O}_9$ to niobium pyrochlores can be explained by the close similarity of the ionic radii of niobium(V) and tantalum(V), and the coincidence of the charge state of cobalt ions. Meanwhile, the cell parameter for the niobium-containing analog of $\text{Bi}_2\text{CoNb}_2\text{O}_9$, according to [25], is much smaller at 10.510 Å. Notably, the unit cell parameter of the magnesium pyrochlore $\text{Bi}_2\text{CoNb}_2\text{O}_9$ is larger at 10.54607 Å [26], compared

to that of the solid solutions $\text{Bi}_2\text{Mg}_{1-x}\text{Co}_x\text{Ta}_2\text{O}_9$ at $x = 0.3$ ($a = 10.5412(8)$ Å) and $x = 0.5$ ($a = 10.5434(8)$ Å). This apparent contradiction can be explained if we assume that a certain fraction of cobalt(II) ions is located in the crystallographic positions of bismuth cations 3. This is favored by the difference in the ionic radii of cobalt(II) ($R(\text{Co(II)})^{\text{h.s.}}_{\text{c.n-6}} = 0.745$ Å) and magnesium (II) ($R(\text{Mg(II)})_{\text{c.n-6}} = 0.72$ Å), and because some of the cobalt ions are oxidized to the Co(III) state, which has a much smaller radius than Co(II). As was shown earlier [17], the presence of bismuth orthotantalate impurities in the samples can be associated with the placement of Co(II) ions, not only in the octahedral sublattice of tantalum(V), but also in the bismuth(III) sublattice, which is due to the higher radius of Co(II) ions than Mg(II). Large cobalt(II) ions are mainly distributed into the octahedral sublattice of tantalum(V), creating oxygen vacancies and causing stress in the octahedral framework due to their low charge and large size.

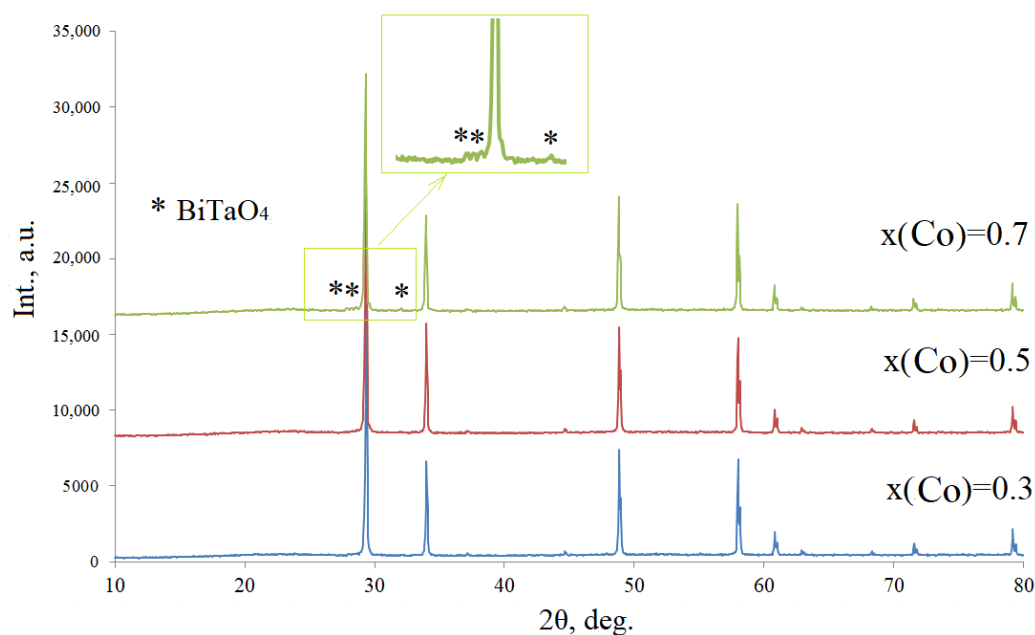


Figure 1. X-ray patterns of $\text{Bi}_2\text{Mg}_{1-x}\text{Co}_x\text{Ta}_2\text{O}_9$ samples at different values of the $x(\text{Co})$ index. Asterisks indicate phase reflections of BiTaO_4 in the X-ray diffraction pattern.

Apparently, to relieve the stress of the octahedral framework, a certain fraction of cobalt(II) ions is distributed into the crystallographic positions of bismuth(III). This distribution requires vacancies in the bismuth sublattice. It can be assumed that vacancies are formed as a result of the formation of bismuth orthotantalate as an impurity phase [17,24]. In most cases, the amount of bismuth orthotantalate is equivalent to the number of 3D ions distributed at the bismuth ion position. In our case, most likely, cobalt(II) ions can be distributed in the bismuth position due to the larger ionic radius of cobalt(II) ions compared to magnesium(II) ions. The need to distribute cobalt in the bismuth position increases with increasing cobalt content in solid solutions, for which the index $x(\text{Co})$ is responsible. Indeed, at $x(\text{Co}) = 0.7$, we observe an impurity phase $-\text{BiTaO}_4$ in the X-ray diffraction patterns of the samples.

According to SEM data (Figure 2), the microstructure of the sample is porous, with partially fused and randomly located elongated grains 1–2 μm in size. As can be seen from the microphotographs, the dependence of the ceramic grain size on the $n(\text{Co})/n(\text{Mg})$ ratio has not been reliably established. We can only state that with an increase in cobalt content, the ceramic grains stick together into larger aggregates, which will lead to an increase in the density of the ceramic as a whole. Local chemical analyses of the samples by EDS show that the experimental qualitative and quantitative composition corresponded to the expected chemical composition (Figure 2).

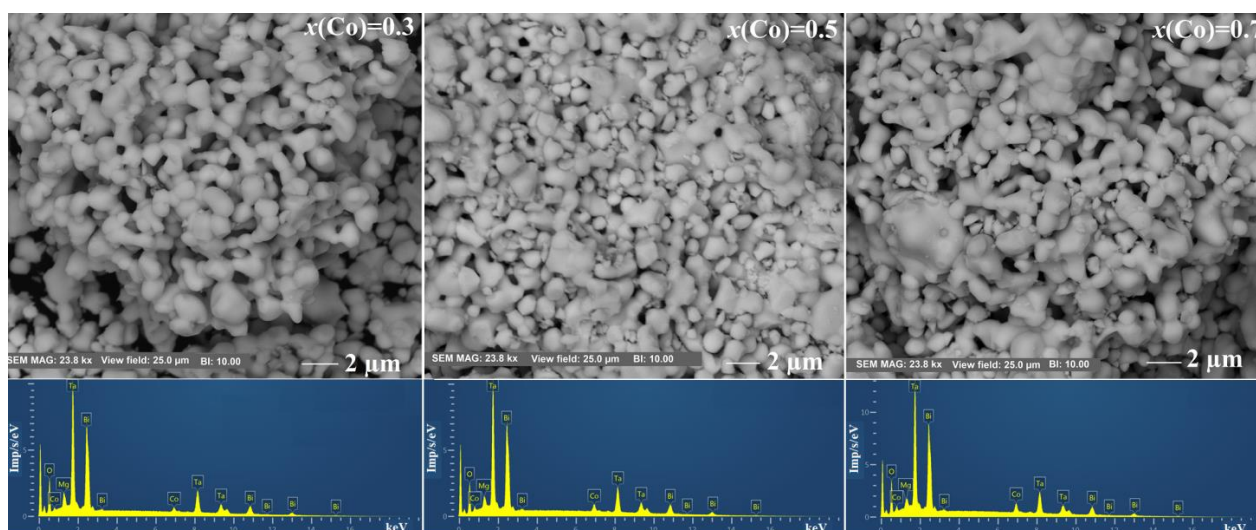


Figure 2. SEM microphotographs of the $\text{Bi}_2\text{Mg}_{1-x}\text{Co}_x\text{Ta}_2\text{O}_9$ at $x(\text{Co}) = 0.3\text{--}0.7$.

3.2. NEXAFS and XPS of the $\text{Bi}_2\text{Mg}_{1-x}\text{Co}_x\text{Ta}_2\text{O}_9$

Figure 3a–f presents XPS Bi5d-, Ta4f-, Ta4d-, Mg1s-, Co2p- and survey spectra of Co,Mg co doped bismuth tantalates with varying Co/Mg ratio, as well as absorption spectra of metal oxide precursors, which were used in the synthesis of $\text{Bi}_2\text{Mg}_{1-x}\text{Co}_x\text{Ta}_2\text{O}_9$ samples. The Mg1s-spectrum also includes the results of decomposition into separate peaks modeled by Gauss–Lorentzian curves, and the background lines modeled by Shirley- or smart-approximation. Table 1 displays the energy positions of the spectra details of $\text{Bi}_2\text{Mg}_{0.5}\text{Co}_{0.5}\text{Ta}_2\text{O}_9$, $\text{Bi}_2\text{MgTa}_2\text{O}_9$ and $\text{Bi}_2\text{CoTa}_2\text{O}_9$. The XPS survey spectra (Figure 3a) exhibit a C1s peak associated with the presence of irremovable surface contamination on the samples. The presence of organic surface contaminants can contribute to the intensity of the O1s peak and affect the reliability of the signal intensity analysis. Therefore, the surface composition of the samples was interpreted based on XPS spectra of bismuth, tantalum and cobalt atoms.

Table 1. The peak energy positions in the XPS spectra of $\text{Bi}_2\text{Mg}_{0.5}\text{Co}_{0.5}\text{Ta}_2\text{O}_9$, $\text{Bi}_2\text{MgTa}_2\text{O}_9$ and $\text{Bi}_2\text{CoTa}_2\text{O}_9$.

Peak	Energy Position (eV)		
	$\text{Bi}_2\text{Mg}_{0.5}\text{Co}_{0.5}\text{Ta}_2\text{O}_9$	$\text{Bi}_2\text{MgTa}_2\text{O}_9$	$\text{Bi}_2\text{CoTa}_2\text{O}_9$
Bi4f _{7/2}	159.05	159.03	158.85
Bi4f _{5/2}	164.38	164.35	164.16
Bi5d _{5/2}	26.08	26.11	25.93
Bi5d _{3/2}	28.98	29.08	28.84
Ta4f _{7/2}	25.59	25.66	25.46
Ta4f _{5/2}	27.49	27.56	27.36
Ta4d _{5/2}	230.08	229.78	230.05
Ta4d _{3/2}	241.02	241.44	241.05
Mg1s	1302.64	1303.19	
Co2p _{3/2}	780.64		780.39
Co2p _{1/2}	796.43		796.18
Co2p _{3/2} sat	785.94		786.01
Co2p _{1/2} sat	801.73		801.80

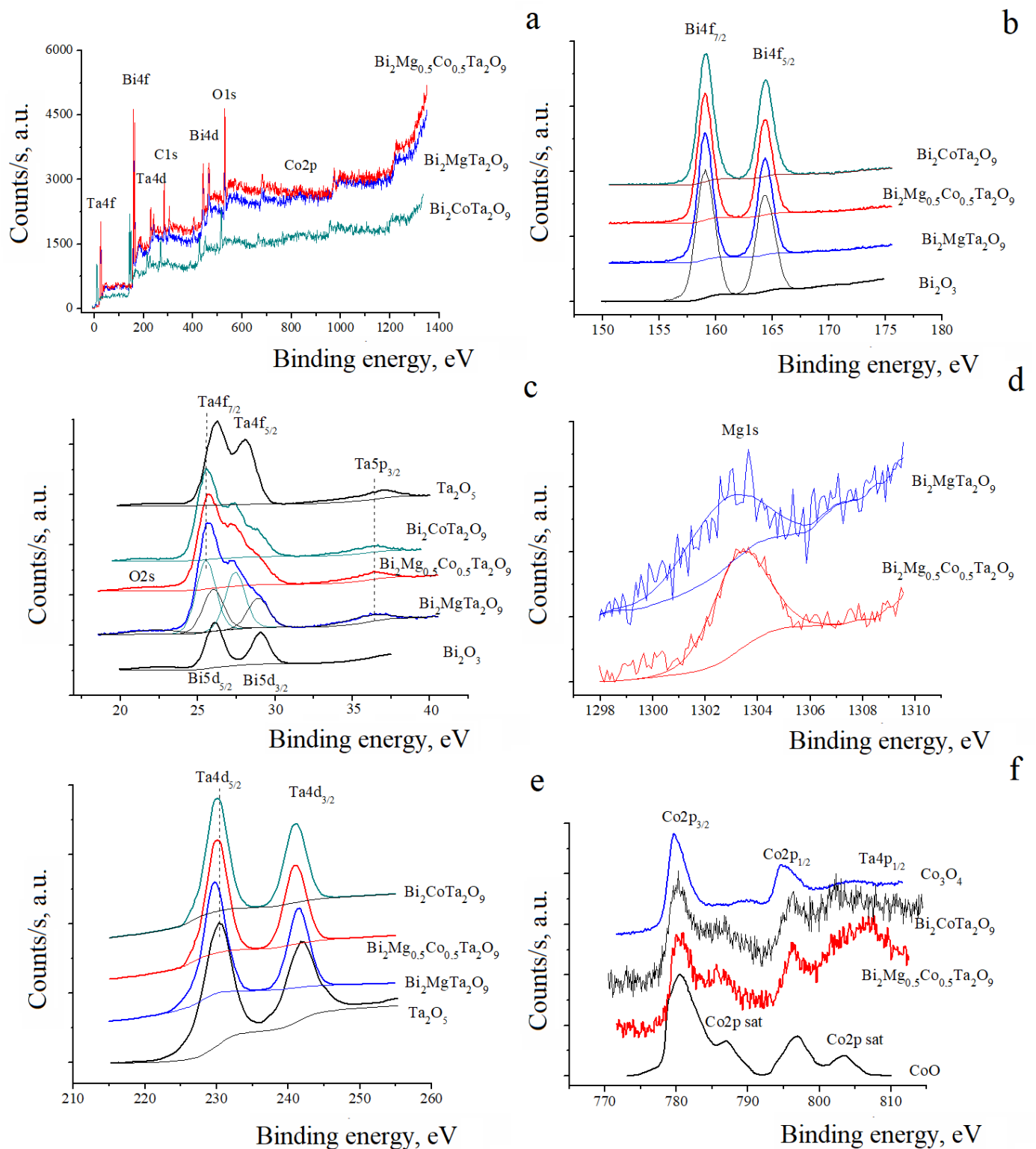


Figure 3. Survey (a), Bi 4f (b) and Ta 4f (c) XPS spectra of $\text{Bi}_2\text{Mg}_{0.5}\text{Co}_{0.5}\text{Ta}_2\text{O}_9$, $\text{Bi}_2\text{MgTa}_2\text{O}_9$, $\text{Bi}_2\text{CoTa}_2\text{O}_9$ and Ta_2O_5 and Bi_2O_3 oxides; Mg 1s (d), Ta 4d and Bi 5d (e); Co 2p XPS spectra of $\text{Bi}_2\text{Mg}_{0.5}\text{Co}_{0.5}\text{Ta}_2\text{O}_9$, $\text{Bi}_2\text{CoTa}_2\text{O}_9$ and Co_3O_4 , CoO oxides (f).

It is important to note that doping the compounds with cobalt and magnesium ions did not significantly affect the spectral characteristics of tantalum, bismuth and magnesium ions. Analysis of XPS Bi4f and Bi5d spectra of solid solutions and bismuth (III) oxide

(Figure 3b,c) shows that the energy position and peak width in the spectra of all samples are nearly identical and correlate well with the corresponding spectra of Bi_2O_3 oxide. The energy position of the peaks in XPS Mg1s spectra (Figure 3d) indicates the presence of divalent magnesium ions [27]. Based on the above, it was concluded that the oxidation state of bismuth and magnesium ions is 3+ and 2+, respectively. Analysis of the XPS Bi5d spectra of the samples revealed a shift of the bands to a low-energy field. It is interesting to note that in the XPS spectra of Bi5d (Figure 3c), the shift of the $\text{Bi}5d_{5/2}$ and $\text{Bi}5d_{3/2}$ absorption bands towards the lower energy is maximal for $\text{Bi}_2\text{CoTa}_2\text{O}_9$ ($\text{Bi}5d_{5/2}$ peak position—25.93 eV) sample compared to $\text{Bi}_2\text{MgTa}_2\text{O}_9$ ($\text{Bi}5d_{5/2}$ peak position—26.11 eV) and $\text{Bi}_2\text{Mg}_{0.5}\text{Co}_{0.5}\text{Ta}_2\text{O}_9$ ($\text{Bi}5d_{5/2}$ peak position—26.08 eV) samples; this indicates that the effective charge of bismuth ions decreased. The decrease in the effective charge of bismuth ions can be explained by the distribution of divalent dopant ions into the crystallographic positions of bismuth.

The largest energy shift is observed for the cobalt composition, while the smallest shift is observed for the magnesium composition, indicating that cobalt ions are more likely to be placed in the bismuth position. The intermediate values of the energy positions for $\text{Bi}5d_{3/2}$ and $\text{Bi}5d_{5/2}$ absorption bands in XPS Bi5d spectra of $\text{Bi}_2\text{Mg}_{0.5}\text{Co}_{0.5}\text{Ta}_2\text{O}_9$ support this conclusion. The conclusion that tantalum ions have the same oxidation state was made on the basis of the undistorted and simple shape of the peaks in the absorption spectra of tantalum. Meanwhile, analysis of the XPS Ta4f, Ta5p and Ta4d spectra of $\text{Bi}_2\text{Mg}_{0.5}\text{Co}_{0.5}\text{Ta}_2\text{O}_9$ samples (Figure 3c,e) showed that the energy positions of the peaks shifted towards lower energies compared to the binding energy in tantalum(V) oxide. The energy shift of the bands in the Ta4f and Ta4d spectra to the low-energy region is $\Delta E = 0.65$ eV and $\Delta E = 0.55$ eV, respectively. The observed shift of the bands indicates that tantalum ions have a lower effective charge $+(5-\delta)$, which may be due to the placement of a certain fraction of heterovalent cobalt and magnesium ions in the octahedral positions of tantalum(V). It is appropriate to note that we observed the effect in the XPS Ta4f and Ta4d spectra of pyrochlores based on bismuth tantalate doped with Cr, Fe, Co, Ni and Cu atoms [18,24]. We explain the energy shift of the bands in the Ta4d and Ta5p spectra of the $\text{Bi}_2\text{Mg}_{0.5}\text{Co}_{0.5}\text{Ta}_2\text{O}_9$, $\text{Bi}_2\text{MgTa}_2\text{O}_9$ and $\text{Bi}_2\text{CoTa}_2\text{O}_9$ samples in a similar way, namely with the replacement of octahedrally coordinated tantalum(V) ions by heterovalent cobalt and magnesium ions. In this case, the $\text{Bi}_2\text{MgTa}_2\text{O}_9$ composition has the lowest energy position of the $\text{Ta}4d_{5/2}$ band at 229.78 eV, which is associated with the lowest effective charge of tantalum ions. XRD analysis shows that only magnesium ions are placed at the tantalum(V) position in $\text{Bi}_2\text{MgTa}_2\text{O}_9$, reducing its effective charge. In this case, the energy shift of the absorption bands for $\text{Bi}_2\text{Mg}_{0.5}\text{Co}_{0.5}\text{Ta}_2\text{O}_9$ and $\text{Bi}_2\text{CoTa}_2\text{O}_9$ samples will be smaller than that observed by the XPS due to the ability of cobalt ions to occupy the bismuth position and have a variable oxidation state other than 2+. This information can be used to analyze the shift of the absorption bands of bismuth(III) and tantalum(V) ions to qualitatively evaluate the distribution of dopant ions.

Now the discussion will move forward to the XPS Co2p spectra (Figure 3f) of $\text{Bi}_2\text{Mg}_{0.5}\text{Co}_{0.5}\text{Ta}_2\text{O}_9$ and $\text{Bi}_2\text{CoTa}_2\text{O}_9$ samples. It is important to note that this spectra energy range includes the peak responsible for the $\text{Ta}4p_{1/2}$ absorption band, which can complicate the cobalt spectra analysis. However, comparing the spectra of the samples with the spectra of Co_3O_4 and CoO [28] shows that the energy position of the main peaks in all the aforementioned spectra is practically identical. The XPS Co 2p spectra of the $\text{Bi}_2\text{Mg}_{1-x}\text{Co}_x\text{Ta}_2\text{O}_9$ and CoO exhibit satellite peaks, which are a characteristic feature of 3D atoms in the divalent state [29]. This suggests that the cobalt atoms in the $\text{Bi}_2\text{Mg}_{1-x}\text{Co}_x\text{Ta}_2\text{O}_9$ samples predominantly have a 2+ charge state.

NEXAFS analysis of Co2p spectra of the $\text{Bi}_2\text{Mg}_{1-x}\text{Co}_x\text{Ta}_2\text{O}_9$ samples at $x(\text{Co}) = 0.5$ and 0.7 and cobalt oxides (Figure 4) leads to a similar conclusion about the charge state of cobalt ions. The spectra of the samples generally correlate with the CoO spectrum, but there are some differences. The spectrum of CoO has energy maximums at 778, 780 and 781 eV. Meanwhile, the complex oxides have a broad diffuse absorption spectrum with a character-

istic peak at 780 eV. The shoulder observed at 781.5 eV may be related to the absorption band characteristic of Co(III) ions, which is also visible in the NEXAFS Co2p-spectrum of Co₃O₄. However, the change in the relative content of Mg/Co atoms in Bi₂Mg_{1-x}Co_xTa₂O₉ samples makes it difficult to clearly determine the Co(II)/Co(III) ions ratio, due to the close proximity of the absorption spectra centers and insufficient signal resolution. It can be concluded that the spectra of samples with different x(Co) are a combination of absorption bands from Co(II) and Co(III) ions. No significant differences were observed between the spectra of Bi₂Mg_{1-x}Co_xTa₂O₉ and Bi₂CoTa₂O₉, and the influence of magnesium ions on the oxidation degree of cobalt was not identified. Based on the X-ray spectroscopy data, it can be concluded that cobalt ions in pyrochlore have a predominantly 2+ oxidation state.

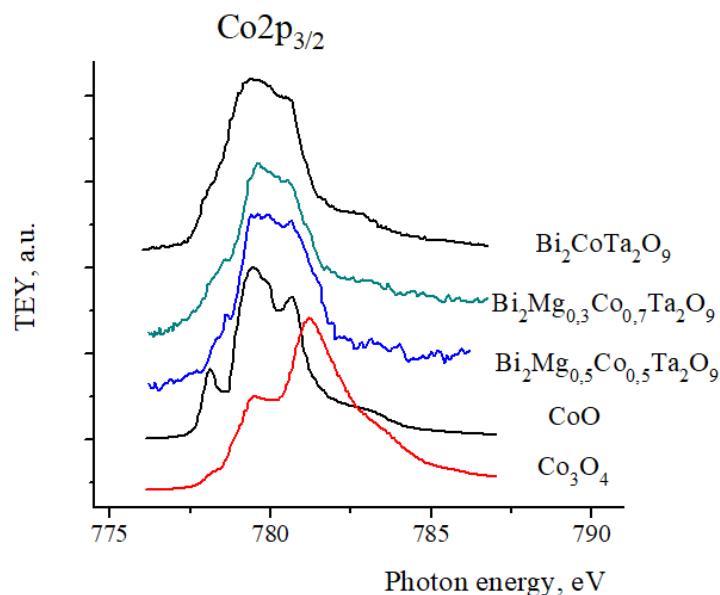


Figure 4. NEXAFS Co2p spectra of Bi₂Mg_{1-x}Co_xTa₂O₉ and cobalt oxides CoO and Co₃O₄.

4. Conclusions

The Bi₂Mg_{1-x}Co_xTa₂O₉ samples crystallize in the pyrochlore structure and are single-phase up to $x < 0.7$. A linear increase in the unit cell parameter of the pyrochlore phase with increasing cobalt content in the samples linearly indicates the formation of solid solutions. In the XPS spectra of the studied samples of solid solutions, a shift in the absorption bands of bismuth ions (Bi4f and Bi5d) to the low-energy region of the spectrum was recorded, which may be due to the placement of a certain fraction of Co(II) ions in the crystallographic positions of bismuth. According to X-ray spectroscopy data, it was established that the oxidation degree of bismuth and magnesium ions is (+3- δ) and (+2), respectively. The absorption band in XPS Ta4f and Ta4d spectra shifted to the lower energy region by the value $\Delta E = 0.65$ eV, and in the region of the Ta4d edge by the value $\Delta E = 0.55$ eV relative to Ta₂O₅, indicating that tantalum ions have the oxidation degree Ta(+5- δ). The results indicate that doping pyrochlores with magnesium ions does not significantly oxidize cobalt ions. Cobalt ions in pyrochlores are primarily in the 2+ oxidation state and to a lesser extent in the 3+ oxidation state. Data from spectroscopic studies show that atoms of transition 3D elements can be distributed over two cationic sublattices, while preferring the octahedral sublattice. The A₂O sublattice is more likely to contain heterovalent ions, such as cobalt(II), which are disproportionate to the ions of the octahedral sublattice (Ta(V)). It has been shown that the structure of pyrochlore contains oxidized ions of transition 3D elements, the proportion of which increases with increasing their total content in the samples. Thus, stabilization of the structure of pyrochlore during heterovalent doping occurs due to the oxidation of part of the transition elements and the placement of incommensurate ions into the sublattice of cations A.

Author Contributions: Conceptualization, N.A.Z.; Funding acquisition, S.V.N.; Investigation, N.A.Z. and S.V.N.; Resources, A.V.K., O.V.P. and B.A.M.; Validation, N.A.Z. and S.V.N.; Visualization, S.V.N., N.A.Z. and B.A.M.; Writing—original draft, N.A.Z. and S.V.N. All authors have read and agreed to the published version of the manuscript.

Funding: The study was supported by the Ministry of Science and Higher Education of Russia under Agreement N 075-15-2021-1351 in part of NEXAFS research.

Data Availability Statement: Data are contained within the article.

Acknowledgments: The XPS studies were performed on the equipment of the Resource Center “Physical methods of surface investigation” of the Scientific Park of St. Petersburg University. The NEXAFS studies were performed on the synchrotron radiation from station “NanoPES” storage ring (National Research Center “Kurchatov Institute”).

Conflicts of Interest: The authors declare no conflict of interest.

References

1. Hiroi, Z.; Yamaura, J.-I.; Yonezawa, S.; Harima, H. Chemical trends of superconducting properties in pyrochlore oxides. *Phys. C Supercond. Appl.* **2007**, *460–462*, 20–27. [[CrossRef](#)]
2. Du, H.; Yao, X. Structural trends and dielectric properties of Bi-based pyrochlores. *J. Mater. Sci. Mater. Electron.* **2004**, *15*, 613–616.
3. Bongers, P.F.; Van Meurs, E.R. Ferromagnetism in Compounds with Pyrochlore Structure. *J. Appl. Phys.* **1967**, *38*, 944–945. [[CrossRef](#)]
4. Greedan, J.E. Frustrated rare earth magnetism: Spin glasses, spin liquids and spin ices in pyrochlore oxides. *J. Alloys Compd.* **2006**, *408–412*, 444–455. [[CrossRef](#)]
5. Giampaoli, G.; Siritanon, T.; Day, B.; Li, J.; Subramanian, M.A. Temperature in-dependent low loss dielectrics based on quaternary pyrochlore oxides. *Prog. Solid State Chem.* **2018**, *50*, 16–23. [[CrossRef](#)]
6. Khaw, C.C.; Tan, K.B.; Lee, C.K. High temperature dielectric properties of cubic bismuth zinc tantalate. *Ceram. Int.* **2009**, *35*, 1473–1480. [[CrossRef](#)]
7. Huiling, D.; Xi, Y. Synthesis and dielectric properties development of new thermal stable bismuth pyrochlores. *J. Phys. Chem. Solids* **2002**, *63*, 2123–2128. [[CrossRef](#)]
8. Subramanian, M.A.; Aravamudan, G.; Subba Rao, G.V. Oxide pyrochlores—A review. *Prog. Solid State Chem.* **1983**, *15*, 55–143. [[CrossRef](#)]
9. McCauley, R.A. Structural Characteristics of Pyrochlore Formation. *J. Appl. Phys.* **1980**, *51*, 290–294. [[CrossRef](#)]
10. Lufaso, M.W.; Vanderah, T.A.; Pazos, I.M.; Levin, I.; Roth, R.S.; Nino, J.C.; Provenzano, V.; Schenck, P.K. Phase formation, crystal chemistry, and properties in the system $\text{Bi}_2\text{O}_3\text{--Fe}_2\text{O}_3\text{--Nb}_2\text{O}_5$. *J. Solid State Chem.* **2006**, *179*, 3900–3910. [[CrossRef](#)]
11. Vanderah, T.A.; Lufaso, M.W.; Adler, A.U.; Levin, I.; Nino, J.C.; Provenzano, V.; Schenck, P.K. Subsolidus phase equilibria and properties in the system $\text{Bi}_2\text{O}_3\text{:Mn}_2\text{O}_3\pm x\text{:Nb}_2\text{O}_5$. *J. Solid State Chem.* **2006**, *179*, 3467–3477. [[CrossRef](#)]
12. Vanderah, T.A.; Siegrist, T.; Lufaso, M.W.; Yeager, M.C.; Roth, R.S.; Nino, J.C.; Yates, S. Phase Formation and Properties in the System $\text{Bi}_2\text{O}_3\text{:2CoO}_{1+x}\text{:Nb}_2\text{O}_5$. *Eur. J. Inorgan. Chem.* **2006**, *2006*, 4908–4914. [[CrossRef](#)]
13. Kamba, S.; Porokhonskyy, V.; Pashkin, A.; Bovtun, V.; Petzelt, J.; Nino, J.C.; Trolier-McKinstry, S.; Lanagan, M.T.; Randall, C.A. Anomalous broad dielectric relaxation in $\text{Bi}_{1.5}\text{Zn}_{1.0}\text{Nb}_{1.5}\text{O}_7$ pyrochlore. *Phys. Rev. B* **2002**, *66*, 054106. [[CrossRef](#)]
14. Nguyen, H.B.; Noren, L.; Liu, Y.; Withers, R.L.; Wei, X.R.; Elcombe, M.M. The disordered structures and low temperature dielectric relaxation properties of two misplaced-displacive cubic pyrochlores found in the $\text{Bi}_2\text{O}_3\text{--MO--Nb}_2\text{O}_5$ (M=Mg,Ni) systems. *J. Solid State Chem.* **2007**, *180*, 2558–2565. [[CrossRef](#)]
15. Ismunandar; Kamiyama, T.; Oikawa, K.; Hoshikawa, A.; Kennedy, B.J.; Kubota, Y.; Kato, K. Static bismuth disorder in $\text{Bi}_{2-x}(\text{CrTa})\text{O}_{7-y}$. *Mater. Res. Bull.* **2004**, *39*, 553–560. [[CrossRef](#)]
16. Zhuk, N.A.; Sekushin, N.A.; Semenov, V.G.; Fedorova, A.V.; Selyutin, A.A.; Krzhizhanovskaya, M.G.; Lutoev, V.P.; Makeev, B.A.; Kharton, V.V.; Sivkov, D.N.; et al. Dielectric properties, Mössbauer study, ESR spectra of $\text{Bi}_2\text{FeTa}_2\text{O}_{9.5}$ with pyrochlore structure. *J. Alloys Compd.* **2022**, *903*, 163928. [[CrossRef](#)]
17. Zhuk, N.A.; Krzhizhanovskaya, M.G.; Sekushin, N.A.; Sivkov, D.V.; Abdurakhmanov, I.E. Crystal structure, dielectric and thermal properties of cobalt doped bismuth tantalate pyrochlore. *J. Mater. Res. Technol.* **2023**, *22*, 1791–1799. [[CrossRef](#)]
18. Zhuk, N.A.; Krzhizhanovskaya, M.G.; Sekushin, N.A.; Kharton, V.V.; Koroleva, A.V.; Nikipelov, S.V.; Sivkov, D.V.; Sivkov, V.N.; Makeev, B.A.; Lebedev, A.M.; et al. Novel Ni-Doped Bismuth–Magnesium Tantalate Pyrochlores: Structural and Electrical Properties, Thermal Expansion, X-ray Photoelectron Spectroscopy, and Near-Edge X-ray Absorption Fine Structure Spectra. *ACS Omega* **2021**, *6*, 23262–23273. [[CrossRef](#)] [[PubMed](#)]
19. Chon, M.P.; Tan, K.B.; Khaw, C.C.; Zainal, Z.; Taufiq-Yap, Y.H.; Chen, S.K.; Tan, P.Y. Subsolidus phase equilibria and electrical properties of pyrochlores in the $\text{Bi}_2\text{O}_3\text{--CuO--Ta}_2\text{O}_5$ ternary system. *J. Alloys Compd.* **2016**, *675*, 116–127. [[CrossRef](#)]
20. Youn, H.-J.; Sogabe, T.; Randall, C.A.; Shrout, T.R.; Lanagan, M.T. Phase Relations and Dielectric Properties in the $\text{Bi}_2\text{O}_3\text{--ZnO--Ta}_2\text{O}_5$ System. *J. Am. Ceram. Soc.* **2001**, *84*, 2557–2562. [[CrossRef](#)]

21. Akselrud, L.G.; Grin, Y.N.; Zavalij, P.Y.; Pecharsky, V.K.; Fundamenskii, V.S. CSD-universal program package for single crystal or powder structure data treatment. In Proceedings of the 12th European Crystallographic Meeting, Moscow, Russia, 20–29 August 1989; p. 155.
22. Zhou, D.; Fan, X.Q.; Jin, X.W.; He, D.W.; Chen, G.H. Structures, Phase Transformations, and Dielectric Properties of BiTaO₄ Ceramics. *Inorg. Chem.* **2016**, *55*, 11979–11986. [[CrossRef](#)] [[PubMed](#)]
23. Shannon, R.D. Revised effective ionic radii and systematic studies of interatomic distances in halides and chalcogenides. *Acta Crystallogr. A* **1976**, *32*, 751–767. [[CrossRef](#)]
24. Zhuk, N.A.; Krzhizhanovskaya, M.G.; Koroleva, A.V.; Nekipelov, S.V.; Sivkov, D.V.; Sivkov, V.N.; Lebedev, A.M.; Chumakov, R.G.; Makeev, B.A.; Kharton, V.V.; et al. Spectroscopic characterization of cobalt doped bismuth tantalate pyrochlore. *Solid State Sci.* **2022**, *125*, 106820. [[CrossRef](#)]
25. Piir, I.V.; Prikhodko, D.A.; Ignatchenko, S.V.; Schukariov, A.V. Preparation and structural investigations of the mixed bismuth niobates, containing transition metals. *Solid State Ion.* **1997**, *101–103*, 1141–1146. [[CrossRef](#)]
26. Zhuk, N.A.; Krzhizhanovskaya, M.G.; Sekushin, N.A.; Kharton, V.V.; Makeev, B.A.; Belyy, V.A.; Korolev, R.I. Dielectric performance of pyrochlore-type Bi₂MgNb_{2–x}Ta_xO₉ ceramics: The effects of tantalum doping. *Ceram. Int.* **2021**, *47*, 19424–19433. [[CrossRef](#)]
27. Khairallah, F.; Glisenti, A. XPS Study of MgO Nanopowders Obtained by Different Preparation Procedures. *Surf. Sci. Spectra* **2006**, *13*, 58–71. [[CrossRef](#)]
28. Hassel, M.; Freund, H.-J. High resolution XPS study of a thin CoO(111) film grown on Co(001). *Surf. Sci. Spectra* **1996**, *4*, 273–278. [[CrossRef](#)]
29. Moulder, J.F. *Handbook of X-ray Photoelectron Spectroscopy: A Reference Book of Standard Spectra for Identification and Interpretation of XPS Data*; Perkin-Elmer Corporation: Eden Prairie, MN, USA, 1992; 261p.

Disclaimer/Publisher’s Note: The statements, opinions and data contained in all publications are solely those of the individual author(s) and contributor(s) and not of MDPI and/or the editor(s). MDPI and/or the editor(s) disclaim responsibility for any injury to people or property resulting from any ideas, methods, instructions or products referred to in the content.